Monthly Notices of the ROYAL ASTRONOMICAL SOCIETY
MNRAS Advance Access published October 31, 2013
MNRAS (2013) doi:10.1093/mnras/stt1902

Non-linear redundancy calibration

Visweshwar Ram Marthi* and Jayaram Chengalur*

National Centre for Radio Astrophysics, Tata Institute of Fundamental Research, Post Bag 3, Ganeshkhind, Pune 411007, India

Accepted 2013 October 4. Received 2013 October 3; in original form 2013 May 20

ABSTRACT

For radio interferometric arrays with a sufficient number of redundant spacings the multiplicity of measurements of the same sky visibility can be used to determine both the antenna gains as well as the true visibilities. Many of the earlier approaches to this problem focused on linearized versions of the relation between the measured and the true visibilities. Here, we propose to use a standard non-linear minimization algorithm to solve for both the antenna gains as well as the true visibilities. We show through simulations done in the context of the ongoing upgrade to the Ooty Radio Telescope that the non-linear minimization algorithm is fast compared to the earlier approaches. Further, unlike the most straightforward linearized approach, which works with the logarithms of the visibilities and the gains, the non-linear minimization algorithm leads to unbiased solutions. Finally, we present error estimates for the estimated gains and visibilities. Monte Carlo simulations establish that the estimator is indeed statistically efficient, achieving the Cramér–Rao bound.

Key words: methods: numerical – methods: statistical – techniques: interferometric.

1 INTRODUCTION

The 'visibilities' obtained by radio interferometers have to be corrected for the unknown gains of the antennas along the signal path before they can be used to image the sky. This is a well-known problem (viz. 'calibration') and calibration routines are available in several different interferometric data reduction packages. A special case of calibration arises when the array is such that a given antenna spacing is present multiple times. Each baseline in such a 'redundant' baseline set measures the same Fourier component of the sky brightness distribution. The only differences between the copies are due to the different multiplicative gains and additive noise along the different signal paths. For a sufficiently redundant array, this multiplicity of measurements of the same physical quantity allows simultaneous estimation of both the antenna gains as well as the true sky visibilities. Some of the earliest work on 'redundancy calibration' was done in the context of the Westerbork Synthesis Radio Telescope (Noordam & de Bruyn 1982; Wieringa 1991, 1992). Interest in redundancy calibration has been revived in the recent past because a number of new instruments [e.g. the Low Frequency Array (LOFAR), Falcke et al. (2006) and the Murchison Widefield Array (MWA), Lonsdale et al. (2009)] have some degree of redundancy at certain scales, to exploit specific engineering advantages. The LOFAR stations, for instance, have a redundant $N \times N$ geometry that allows accurate calibration of each of the antennas within the station (Noorishad et al. 2012; Wijnholds & Noorishad 2012). Further, certain astrophysics and cosmology experiments would benefit from redundant configurations for the telescope geometry: the cylinder array (Peterson, Bandura & Pen 2006) and the Baryon Acoustic Oscillation Broadband and Broad-beam (BAOBAB) array (Pober et al. 2012) are specific examples, while Parsons et al. (2012) discuss redundant configurations for redshifted 21cm studies such as the epoch of reionization.

Many of the algorithms in previous work in redundancy calibration largely used linear least-squares (LLS) algorithms to solve for the antenna gains and sky visibilities. In this paper, we apply a simple non-linear least-squares (NLS) minimization algorithm and compare its performance against that of the LLS algorithms. This is done using simulated data, with the simulations being done in the context of an ongoing upgrade of the Ooty Radio Telescope (ORT). We also compute error estimates on the derived solutions, and compare the accuracy of these estimates against ensemble average errors derived from a Monte Carlo simulation and the Cramér–Rao bound (CRB).

2 REDUNDANCY CALIBRATION

At any instant of time, a two-element interferometer measures a single Fourier mode (called the visibility) of the incident radiation field. The (complex) gains along each of the signal paths and the additive thermal noise cause the measured visibility to differ from the true visibility. Mathematically

$$V_{ij} = g_i g_j^* M_{ij} + N_{ij}, \quad (1)$$

* E-mail: vrmarthi@ncra.tifr.res.in (VRM); chengalur@ncra.tifr.res.in (JC)

where g_i and g_j are the complex gains associated with the antennas i and j, respectively, M_{ij} is the true visibility of the sky corresponding to the baseline between antennas i and j, and N_{ij} is the complex-valued additive noise. For the sake of clarity, we ignore other factors such as the primary beam of the (assumed identical) antennas and polarization leakage which would also cause the measured visibility to differ from the true one (see e.g. Thompson, Moran & Swenson 2001). We also assume that phase variations arising from the ionosphere can be lumped together with the complex gain of the receiver chain, and that the correlator does not introduce any baseline based gains or errors. We return to a discussion of these assumptions in Section 4.2.

In order to recover the true visibility, the gains g_i would have to be known, i.e. the interferometer would have to be calibrated. Conceptually, the simplest way to do this would be to observe a region of the sky where the true visibilities M_{ij} are known (viz. a *calibrator* source), and use the observed V_{ij} to solve for the gains. If the gain variation time-scale is long compared to the time interval between observations of calibrator sources, the solutions can be interpolated in time to obtain the gains at some intermediate time, for example a time when the *target* source, whose true visibilities one would like to estimate, is being observed. For a multi-element interferometer with N elements, the number of instantaneous visibility measurements go like $\sim N^2$, while the number of unknown gains are only N. In addition, the measured visibilities must obey the amplitude and phase closure constraints. As is well known, these facts can be used to iteratively refine both the gains and the visibilities (viz. do *self*-calibration), provided some reasonable initial guess for the gains and the structure of the source is available (see e.g. Thompson et al. 2001).

Another interesting case arises when the array is redundant, i.e. there are multiple instances of the same antenna separation. The observed visibilities on these redundant baselines would differ only by the instrumental gains and the additive thermal noise. If there is sufficient redundancy this would allow solving for the unknown antenna gains, as well as the true visibilities (viz. *redundancy* calibration), essentially independent of any assumed model for the sky (see e.g. Cornwell & Fomalont 1999). Redundancy calibration algorithms discussed in the literature are broadly based on LLS methods. One such example is the LLS algorithm proposed by Noordam & de Bruyn (1982). We give a brief description below, and direct the interested reader to the longer discussion in the paper cited above and those of Wieringa (1991, 1992) and Liu et al. (2010).

Ignoring the noise term N_{ij} and taking logarithm of equation (1) we get

$$\ln|V_{ij}| = \ln|g_i| + \ln|g_j| + \ln|M_{|i-j|}| \tag{2}$$

$$\angle V_{ij} = \angle g_i - \angle g_j + \angle M_{|i-j|}. \tag{3}$$

The above system of equations can be written in the familiar matrix form

$$\boldsymbol{y} = \mathbf{A}\,\boldsymbol{x} \tag{4}$$

separately for the amplitude and the phase equations, where $\boldsymbol{y}$ is a column vector containing the (amplitudes or phases of the) observed visibilities on all the redundant baselines, $\boldsymbol{x}$ is a column vector containing the antenna gains and the true visibilities on those baselines (with the dimension of $\boldsymbol{x}$ being significantly smaller than the dimension of $\boldsymbol{y}$) and $\mathbf{A}$ is a sparse matrix depending only on the array geometry. For example, for a uniformly spaced linear N-element array, $\boldsymbol{y}$ is of length $N(N-1)/2-1$ while the length of $\boldsymbol{x}$ is $N+(N-2)$. Specifically, for the amplitude equation (2):

$$\boldsymbol{y} = \begin{bmatrix} \ln|V_{1,2}| \\ \ln|V_{1,3}| \\ \ln|V_{1,4}| \\ \vdots \\ \ln|V_{n-1,n}| \end{bmatrix}, \qquad \boldsymbol{x} = \begin{bmatrix} \ln|g_1| \\ \ln|g_2| \\ \ln|g_3| \\ \vdots \\ \ln|g_n| \\ \ln M_{|1|} \\ \vdots \\ \ln M_{|n-2|} \end{bmatrix} \tag{5}$$

and

$$\mathbf{A} = \begin{bmatrix} 1 & 1 & 0 & \cdots & 1 & 0 & \cdots & 0 & 0 \\ 1 & 0 & 1 & \cdots & 0 & 1 & \cdots & 0 & 0 \\ 1 & 0 & 0 & 1 & \cdots & 0 & \cdots & 0 & 0 \\ \vdots & & & & \ddots & & & \vdots & \\ 0 & 0 & \cdots & 1 & 1 & 0 & 1 & 0 & 0 \\ 0 & 0 & \cdots & 1 & 0 & 1 & 0 & 0 & 0 \\ 0 & 0 & \cdots & 0 & 1 & 1 & 1 & 0 & 0 \end{bmatrix}. \tag{6}$$

For the phase part of the solution, some elements of the matrix $\mathbf{A}$ undergo a sign change corresponding to the complex conjugation of one of the gains, without the structure of the matrix itself being altered. As can be seen, the matrix $\mathbf{A}$ is highly sparse, leading to fast computation of the solution

$$\boldsymbol{x} = \mathbf{A}^{-1}\,\boldsymbol{y} \tag{7}$$

in a single step separately for the amplitudes and the phases. We clarify that by $\mathbf{A}^{-1}$ we mean the generalized inverse $(\mathbf{A}^{\mathrm{T}}\mathbf{A})^{-1}\mathbf{A}^{\mathrm{T}}$. Since the matrix $\mathbf{A}$ is static, its inverse has to be computed only once, after which it can be used for all time intervals at which the redundancy calibration needs to be done.

While this method is straightforward to implement, it ignores the additive noise, and hence is suitable only in high signal-to-noise ratio (SNR) situations. Liu et al. (2010) discuss the problems that arise if this algorithm is used in the low SNR regime, and suggest an alternative algorithm. Their method is based on linearizing the equations by considering a Taylor series expansion of the complex exponentials in equation (1).

Following a Taylor series expansion and approximation to the linear term, the complex gains and visibilities can be rewritten as

$$g_i = g_i^0[1 + \Delta\eta_i + i\phi_i] \tag{8}$$

$$g_j = g_j^0[1 + \Delta\eta_j + i\phi_j] \tag{9}$$

$$M_{|i-j|} = M^0_{|i-j|}[1 + \Delta\zeta_{|i-j|} + i\theta_{|i-j|}] \tag{10}$$

$$V_{ij} = V_{ij}^0[1 + \rho_{ij} + i\psi_{ij}] \tag{11}$$

$$\delta_{ij} = V_{ij} - V_{ij}^0, \tag{12}$$

where

$$V_{ij}^0 = g_i^0 g_j^0 M^0_{|i-j|}. \tag{13}$$

The superscript denotes the fiducial guess for the various quantities that has to be provided at the start of the algorithm. Finally, the reduced expression for the correction term reads as

$$\delta_{ij} = V_{ij}^0[\Delta\eta_i + i\phi_i + \Delta\eta_j - i\phi_j + \Delta\zeta_{|i-j|} + i\theta_{|i-j|}], \tag{14}$$

which can be written in matrix form as

$$\boldsymbol{y} = \mathbf{B}\,\boldsymbol{x} \tag{15}$$

Unlike the earlier case the amplitude and phase equations are coupled. Further, unlike the matrix $\mathbf{A}$, which depends only on the geometry of the array, the matrix $\mathbf{B}$ depends on both the geometry of the array and the current estimate of the gains and true visibilities. It hence has to be updated and a fresh pseudo-inverse computed for each iteration. Note also that one has to supply the fiducial solutions g_i^0 and $M_{|i-j|}^0$ at the start.

Both the methods outlined above lend themselves to straightforward implementation using any one of the several available linear algebra libraries. Another recent algorithm of interest is the Weighted Alternating Least Squares (WALS) algorithm proposed by Wijnholds & Noorishad (2012) (also see Wijnholds 2010). The antenna gains and phases are obtained as the solutions that minimize the covariance matched weighted differences between the measured and the estimated visibilities

$$\left\{\widehat{\boldsymbol{g}}, \widehat{\mathbf{M}}_0, \widehat{\sigma_n}\right\} = \underset{\widehat{g},\,\widehat{\mathbf{M}}_0,\,\widehat{\sigma_n}}{\arg\min} \left\|\mathbf{W}_c\left(\widehat{\mathbf{V}} - \mathbf{G}\,\mathbf{M}_0\mathbf{G}^H - \boldsymbol{\Sigma}_n\right)\boldsymbol{W}_c\right\|^2, \tag{16}$$

where $\widehat{\boldsymbol{g}}$ is the vector of the antenna gains to be estimated and $\mathbf{G}$ is the diagonal matrix of the gains. $\widehat{\mathbf{M}}_0$ is the Toeplitz matrix of the true visibilities (to be estimated) of all baselines obtained from the compact set of visibilities $\mathbf{M}$ from the unique baselines. $\widehat{\sigma_n}$ is the noise power vector to be estimated and Σ_n is the diagonal noise covariance matrix. The weighting factor is chosen as $\mathbf{W}_c = \mathbf{V}^{-1/2}$, where $\mathbf{V}$ is the matrix of the measured visibilities. A model is assumed initially to estimate the gains $\boldsymbol{g}$ from an eigenvalue decomposition. In the next step, these gains are used to estimate the visibilities $\mathbf{M}_0$. The procedure is repeated iteratively until a suitable convergence criterion is satisfied to obtain the estimates $\widehat{\boldsymbol{g}}$ and $\widehat{\mathbf{M}}_0$.

The first two methods outlined above estimate the amplitudes and phases of the gains and the visibilities. However, the steepest descent algorithm based on NLS minimization, described below, estimates the gains and the visibilities directly as common numbers on the Argand plane. The phases hence estimated are found to be free from the errors inherent in the logarithmic method or the linearized method of Liu et al. (2010), where they are found to be unreliable when large. However, alignment of the amplitudes and phases would still require external calibration as explained below. Besides, all the above three methods use matrix inversion, resulting in N^4 operations. However, the WALS method suggested by Wijnholds & Noorishad (2012) is capable of exploiting the redundant structure of the problem thereby achieving N^2 complexity, putting it on par with the steepest descent method described below.

3 STEEPEST DESCENT REDUNDANCY CALIBRATION

In the general case of arrays with arbitrary geometry, equation (1) is routinely solved for the unknown antenna gains using NLS minimization algorithms. It seems reasonable hence to try a similar method in the redundancy calibration case, with the difference being that one would solve not only for the unknown antenna gains, but also for the unknown true visibilities.

We begin by defining a real-valued objective function

$$\Lambda = \sum_i \sum_{j>i} w_{ij} \left\| \left(V_{ij} - g_i g_j^* M_{|i-j|}\right)\left(V_{ij}^* - g_i^* g_j M_{|i-j|}^*\right) \right\| \tag{17}$$

summed over all baselines, where w_{ij} is a real-valued weight. We aim to minimize the objective function Λ with respect to the complex-valued gains $\boldsymbol{g}$ *and* the true sky visibilities $\boldsymbol{M}$.

For brevity, henceforth we call the vector $[\boldsymbol{g}\ \boldsymbol{M}]$ the parameter vector $\boldsymbol{\Theta}$.

$$\boldsymbol{\Theta} = [\boldsymbol{g}\ \boldsymbol{M}] = \left[\ g_1,\ g_2,\ \ldots\ g_N,\ \ M_{|1|},\ M_{|2|},\ \ldots\ M_{|L|}\ \right]$$

corresponding to a redundant array consisting of N antennas and L redundant baselines. The solutions $\widehat{\boldsymbol{\Theta}}$, being the estimates of $\boldsymbol{\Theta}$ that minimize Λ, are those at which the derivatives of Λ with respect to the elements of $\boldsymbol{\Theta}$ vanish uniformly, i.e.

$$\frac{\partial \Lambda}{\partial g_k} = 0 \ \ \forall\, k \in \{\ 1, 2, \ldots, N\ \} \tag{18}$$

and

$$\frac{\partial \Lambda}{\partial M_{|k-j|}} = 0 \ \ \forall\, k-j \in \{\ 1, 2, \ldots, L\ \}. \tag{19}$$

These equations yield, upon some algebraic manipulation, the solutions

$$g_k = \frac{\sum\limits_{j\neq k} w_{kj} g_j M_{|k-j|}^* V_{kj}}{\sum\limits_{j\neq k} w_{kj} |g_j|^2\ |M_{|k-j|}|^2} \tag{20}$$

and

$$M_{|k-j|} = \frac{\sum\limits_{j>k} g_k^* g_j V_{kj}}{\sum\limits_{j>k} w_{kj} |g_k|^2 |g_j|^2}, \tag{21}$$

where the sum is taken over the appropriate redundant baseline sets.

Note that equations (20) and (21) involve the (unknown) true gains and visibilities. This circularity can be circumvented by taking an iterative approach to the solution: one takes small steps in the direction of the true solutions, starting from an arbitrary initial guess. The corrective steps have to be taken in the direction of the negative gradient for the most rapid convergence. We redefine quantities in equations (20) and (21) as Q_k and R_{kj}, respectively:

$$Q_k = \frac{\sum\limits_{j\neq k} w_{kj} g_j M_{|k-j|}^* V_{kj}}{\sum\limits_{j\neq k} w_{kj} |g_j|^2\ |M_{|k-j|}|^2} \tag{22}$$

$$R_{kj} = \frac{\sum\limits_{j>k} g_k^* g_j V_{kj}}{\sum\limits_{j>k} w_{kj} |g_k|^2 |g_j|^2} \tag{23}$$

We additionally define a step size $0 < \alpha < 1$ so that the solutions can be obtained iteratively as

$$g_k^{n+1} = (1-\alpha) g_k^n + \alpha {Q_k}^n \tag{24}$$

$$M_{|k-j|}^{n+1} = (1-\alpha) M_{|k-j|}^n + \alpha {R_{kj}}^n. \tag{25}$$

Of course, the rate of convergence will depend upon the value chosen for α: if it is too small (i.e. $\alpha \ll 1$), convergence will be

slow, on the other hand, a large value (i.e. $\alpha \sim 1$) could lead to a situation where the algorithm fails to converge. There are well-known methods [such as, for example, the Levenberg–Marquardt method (see e.g. Press et al. 1992)] for determining the optimal value for α: however, these require computation of the Hessian matrix at each iteration, and are computationally more expensive. In our simulations below, we use a fixed value of α (i.e. $\sim$0.3). While a fixed value for α may not be optimal, it more than compensates for the expenditure of computing the Hessian even if consuming a few more iterations.

We now enumerate the steps involved in steepest descent method for estimating the antenna gains and the sky visibilities using the NLS algorithm given above.

(i) If this is the first time step being solved for, initialize the gains and model visibilities to $\mathbf{\Theta} = [\boldsymbol{g}\ \boldsymbol{M}] = [(1, 0),\ (1, 0),\ (1, 0),\ \ldots (1, 0)]$. Otherwise set them to the solutions obtained for the last time step. Set the weights w appropriately based on the system temperature. (In the simulation described below we set them all uniformly to unity). Choose an ϵ for the convergence criterion (set to $\epsilon = 0.005$ in our simulations).

(ii) Integrate the correlated signal from each antenna pair, i.e. the visibility from each baseline $V_{ij}\ \forall\, i, j \in 1, 2, \ldots N, j > i$, for the specified time interval.

(iii) Using the available $\mathbf{\Theta} = [\boldsymbol{g}\ \mathbf{M}]$ and w, compute each Q_k and R_{kj} using expressions (22) and (23).

(iv) Update the gains $\boldsymbol{g}$ and the visibilities $\mathbf{M}$ using equations (24) and (25).

(v) Compute the fractional change in each element of $\boldsymbol{g}$ and $\mathbf{M}$. If the largest fractional change is $>\epsilon$ go to step (iii) else stop.

In the case of routine interferometric calibration, the visibilities $M_{|k-j|}$ are known, and hence there is only one equation to work with, viz. (24). We point out in passing a further similarity with the calibration of non-redundant arrays. Consider the fundamental equation (1) which we rewrite here for the redundant array, ignoring the additive noise term.

$$V_{ij} = g_i g_j^* M_{|i-j|}. \tag{26}$$

Scaling $g_i g_j^*$ by some complex constant z_k while simultaneously scaling $M_{|i-j|}$ by $1/z_k$ leaves the equation unchanged. This is the well-known ambiguity problem of self-calibration (Hamaker 2000). Equivalently, in the redundant calibration solution, the gain amplitudes are determinable only up to an overall scalefactor (and the visibility amplitudes to the inverse square of this scalefactor). Similarly, the gain phases are determinable only up to a linear gradient (and the visibility phases to the negative of this gradient). In this respect, redundancy calibration is analogous to self-calibration. In the simulations described below, we use the known input source positions and the known input source fluxes to determine the overall scalefactor and phase gradient. In practice, these overall scalefactors would have to be determined by some external calibration. Other proposed ways to resolve these ambiguities (see e.g. the discussion in Wijnholds & Noorishad 2012) are to apply the following constraints to the solutions

$$\sum_{n=1}^{N} g_n = g_c, \quad \sum_{n=1}^{N} \phi_n = 0, \quad \sum_{n=1}^{N} \boldsymbol{r_n}\phi_n = 0, \tag{27}$$

where g_c is some mean gain known a priori, g_n and ϕ_n are the antenna gain amplitude and phase, respectively, and $\boldsymbol{r_n}$ is the position vector of the nth element in the array. In the case of the ORT, where the telescope is equatorially mounted, and the baseline lengths do not change with time, resolving these ambiguities by external calibration and the requirement that the gain solutions vary slowly but that the visibility solutions are constant with time is relatively more simple.

4 SIMULATIONS

4.1 Description

The simulations were done in the context of the ongoing upgrade of the ORT. The ORT is an offset parabolic cylinder with its long axis parallel to the rotation axis of the earth (Swarup et al. 1971). The cylinder is fed by a linear phased dipole array. As part of the upgrade the signals from these dipoles are digitized and then fed to a correlation receiver, greatly enhancing the instantaneous field of view and sensitivity of the telescope. More details of the upgrade and the design of the new receiver system can be found in Prasad & Subrahmanya (2011).

The redundancy calibration algorithms were checked against simulated data from the upgraded ORT. The simulator forms a part of a suite of programs intended to become an integrated software package for analysis of data from the upgraded telescope. The simulator generates the expected visibilities from a variety of sources including (a) a point source at the phase centre (b) a collection of point sources randomly distributed within the field of view and (c) a sky source distribution that follows the known source counts at the frequency of operation of the telescope, viz. 325 MHz (Rengelink et al. 1997). Since the ORT is oriented in the north–south direction and is equatorially mounted, the projected baseline lengths between the feed dipole elements do not vary when tracking the source. A suitable coordinate system to work in is hence one in which the U-axis is oriented east–west, the V-axis north–south and the W-axis chosen appropriately as to complete a right-handed Cartesian system. Sky positions would, as usual, be expressed in terms of the corresponding direction cosines (l, m, n). In such a coordinate system, it is easy to show that the visibility corresponding to a pair of feed dipoles separated by a distance $v = d/\lambda$ for a point source of flux S and equatorial coordinates (α_0, δ_0) is

$$V(u, v, w) = V(0, v, 0) = S.\mathrm{e}^{\mathrm{i}2\pi vm} = S.\mathrm{e}^{\mathrm{i}2\pi d \cos\delta_0/\lambda}. \tag{28}$$

We note that although the simulations have been done in the specific context of the ORT, the non-linear steepest descent algorithm is generic and applicable to any redundant array. In the figure and results presented below we use a redundant configuration with up to 40 stations (as appropriate for Phase I of the ORT upgrade; see Prasad & Subrahmanya 2011). However, we have also run the simulations for arrays with as few as five stations, and find that the NLS algorithm works well even in such situations. For all the simulations, Gaussian noise appropriate to the system temperature, radio frequency bandwidth and integration time was added to the model visibilities. These simulated visibilities then formed the input to the different redundancy calibration algorithms.

The matrices $\mathbf{A}$ and $\mathbf{B}$ in the Wieringa (1992) and Liu et al. (2010) algorithms are sparse and often singular: techniques like QR decomposition or singular value decomposition would hence have to be used to solve the corresponding matrix equations. In our implementation, we have used matrix calls from the GNU Scientific Library (GSL). In the non-linear method, as described above, we iterate the equations (24) and (25).

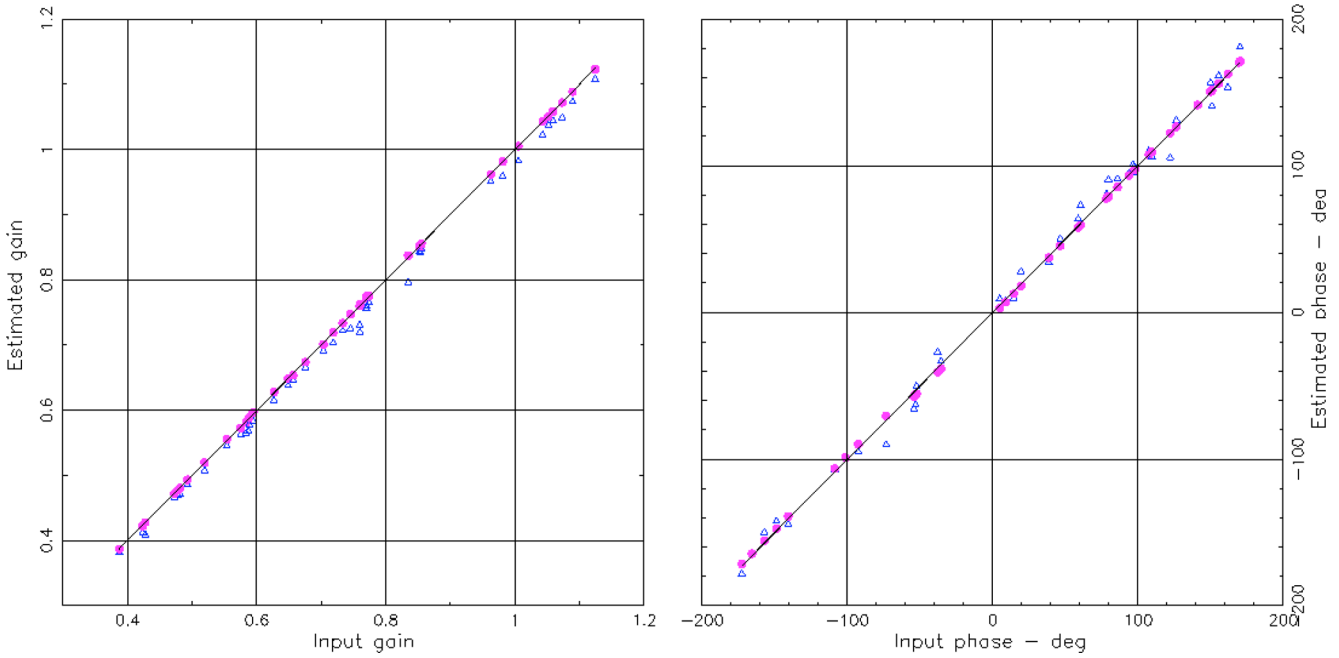

Figure 1. The comparison between the antenna gain amplitudes and phases as estimated by the logarithmic method of Wieringa (1992) and the NLS method is described here. The SNR per visibility is 10, and the input model is the simplest possible, viz. a single source at the phase centre. The solid line represents the ideal situation where the estimated values are equal to the input values. As can be seen, even for this simple model and at this relatively good SNR, the logarithmic method gives biased estimates, shown here as the open circles. In contrast, the NLS estimates, shown by the filled triangles, are not biased. Liu et al. (2010) discuss a linearized logarithmic method which removes this bias, but which is computationally significantly more expensive.

4.2 Results and discussion

Fig. 1 shows the antenna gains and phases estimated from a run of the logarithmic redundancy calibration algorithm of Wieringa (1992), compared against the same numbers estimated from a run of the NLS algorithm, for an SNR per visibility of 10. Although the NLS algorithm works well and provides unbiased solutions for a realistic sky model, this figure is shown here purposefully for the simplest input model, i.e. a point source at the phase centre, so as to illustrate the bias on the gains and phases at uniform SNRs on all baselines. It can be seen that despite a reasonable SNR and a simple sky model, the logarithmic method gives biased estimates. As described above, the principal aim of the Liu et al. (2010) method was to eliminate this bias, and in their paper they show results to validate that their method indeed does avoid the bias. In our implementation too, we find that the Liu et al. (2010) method gives unbiased results; however, for clarity we have shown only results from the NLS method and the Wieringa (1992) method in Fig. 1. From the figure, it is clear that the NLS estimates are unbiased as well. To illustrate further the quality of the NLS solutions we show in Fig. 2 the results from a simulation in which the antenna gains and sky visibilities were kept fixed from run to run, but each run had independent noise added to the simulated visibilities. The visibilities themselves corresponded to a model sky with a source population that matches that expected from the source counts at 325 MHz. The figure shows the known input parameters to the simulation as well as the mean and rms (computed over the different runs, i.e. the ensemble rms) of the estimated parameters. The rms has been scaled by a factor of 10 for the gains and 5 for the visibilities so that they can be seen clearly in the plot. As can be seen, the NLS algorithm does an excellent job of recovering the parameters.

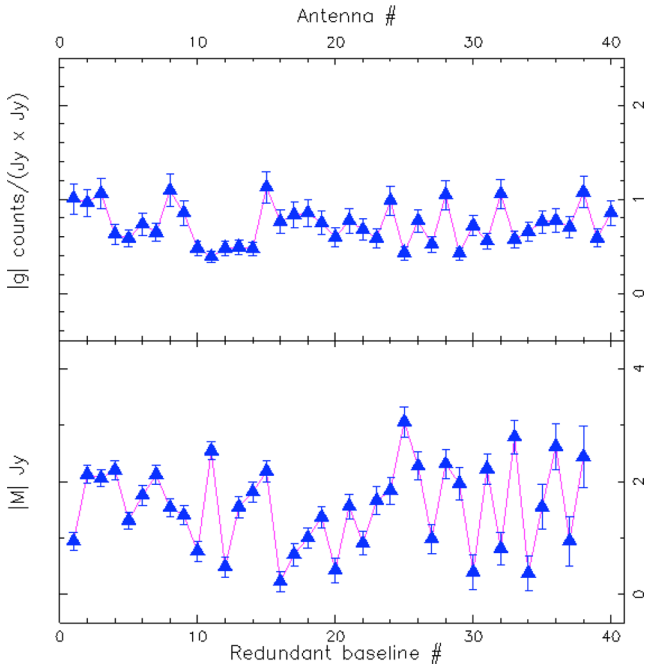

Figure 2. The solutions, with their error bars obtained from a Monte Carlo simulation for a realistic sky model, are shown here. The SNR for a 2 Jy radio source is 4, which can be considered to be the mean SNR over all baselines. The upper panel shows the amplitudes of the gains and the lower panel shows the visibilities. The solid line connects the true solutions and the filled triangles are the estimated solutions. The error bars on the estimated gains have been magnified by a factor of 10 and those on the estimated visibilities by a factor of 5 to enable them to be seen clearly.

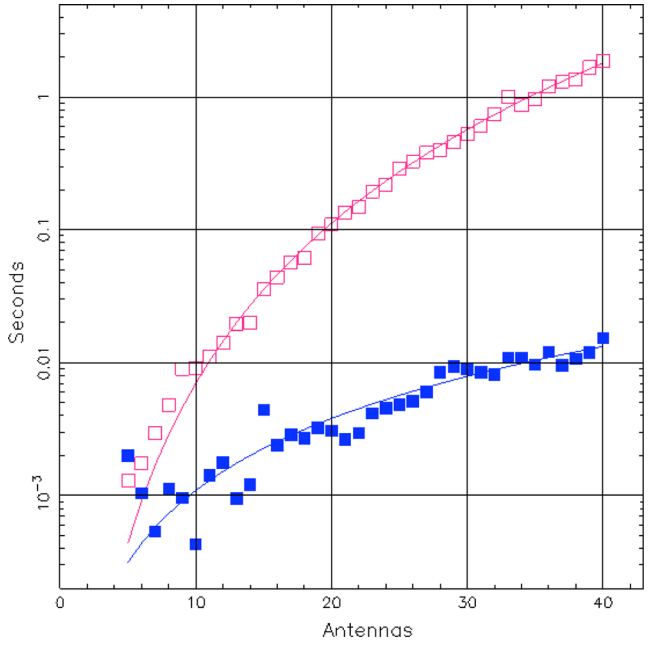

Figure 3. Plot showing the comparison between the time taken for the two algorithms: the linearized method by Liu et al. (2010) and the NLS method described in this paper. The plot shows the time taken by the algorithms (excluding the time taken for disc I/O) as a function of the number of antennas in the array. The sky model is generated from the known source counts at 325 MHz, and the average SNR per visibility is ≈4. The filled squares show the time taken by the NLS algorithm for different number of antennas, and the open squares show the corresponding time taken by linearized method of Liu et al. (2010). The corresponding solid lines show the empirical curves of the form ax^n with $a = 7.0 \times 10^{-7}$, $n = 4.0$ and $a = 8.2 \times 10^{-6}$, $n = 2.0$ for the Liu et al. (2010) and NLS methods, respectively, clearly reflecting the structure of the algorithm.

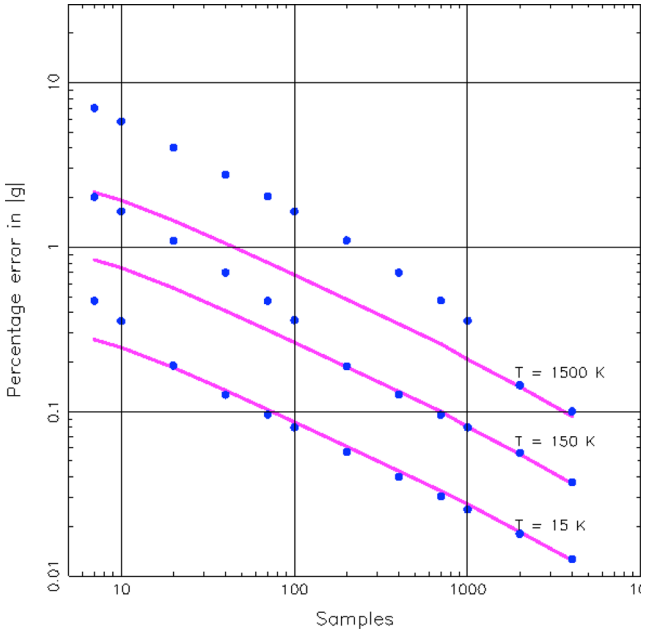

Figure 4. Shows the behaviour of the error on the antenna-averaged gains for three different system temperatures. The filled circles represent ensemble errors obtained from the Monte Carlo run, whereas the solid line is the CRB. At lower system temperatures, the errors reach the CRB upon integration of fewer samples. At $T_{\rm sys} = 1500$ K, for example, many more samples would have to integrated than at $T_{\rm sys} = 150$ K to attain the CRB.

Although the linearized method described in Liu et al. (2010) avoids the bias inherent in the logarithmic methods, it is, as described above, computationally significantly more expensive than the Wieringa (1992) method. Fig. 3 shows the time taken by the Liu et al. (2010) and NLS algorithms as a function of the total number of antennas. The run times exclude the time taken for data I/O from the disc. The linearized algorithm of Liu et al. (2010) clearly shows a N^4 dependence, whereas the NLS[1] algorithm behaves as N^2. Note that there was no explicit multithreading in our implementation, and no compiler optimization was used. The NLS algorithm is significantly faster and is very effective in real-time calibration.

Since calibration is essentially an estimation problem, it is natural to ask what the errors on the estimated parameters (i.e. the gains and visibilities in this case) are, and how the errors obtained via the NLS algorithm compare with fundamental bounds on the error, viz. the CRB. As is well known (see e.g. Press et al. 1992), the covariance matrix Σ_ϑ of the estimated parameters is related to the Hessian matrix $\mathcal{H}$ as

$$\mathcal{H}(\vartheta) = \Sigma_\vartheta^{-1}. \tag{29}$$

Further, if the measurement errors are independent and identically distributed Gaussian noise, then the Hessian matrix is equal to the Fisher information matrix and the variances estimated from the Hessian matrix correspond to the CRB (see e.g. Poor 1994). The parameter errors estimated in this way would hence be a lower bound to the true error. Fig. 4 shows a comparison between the mean ensemble error obtained from the simulations for runs with different system temperatures (i.e. SNR). The ensemble errors attain the CRB when the SNR $\gtrsim 10$.

Finally, in Fig. 5 we show the 'kite plots': the Hessian and covariance matrices. These matrices are clearly diagonally dominant. A good approximation to the variance can hence be obtained quickly by approximating the Hessian matrix to be diagonal. In the simulation described above, this approximation leads to a difference of only ∼1 per cent in the values of the estimated standard deviation. Since the diagonal approximation simplifies the inversion of the Hessian, we could adopt this approximation in the Levenberg–Marquardt algorithm to refine the step size after each iteration. However, since we find that a constant step size is adequate we do not pursue this any further here.

As stated in Section 2 we have been assuming that the beam shapes of the individual antenna elements are identical, and that the ionospheric phases can be lumped together with the electronic gains of the elements. In general, these assumptions are only approximately true. Further, we have been only dealing with a scalar equation, whereas, in the presence of phenomena which mix the two polarizations (e.g. differential faraday rotation across the array, receptors whose response is not perfectly orthogonal, i.e. suffer from 'leakage', 'ellipticity', which themselves could in general vary across the field of view) it is not possible to decouple the calibration of the nominally orthogonal polarizations. High dynamic range imaging would require one to address all of these issues, and there have been a number of algorithms proposed [dubbed '3GC'

[1] The referee of this paper also communicated to us that the NEWSTAR package also uses a steepest descent method which leads to N^2 performance when the structure of the problem is properly exploited.

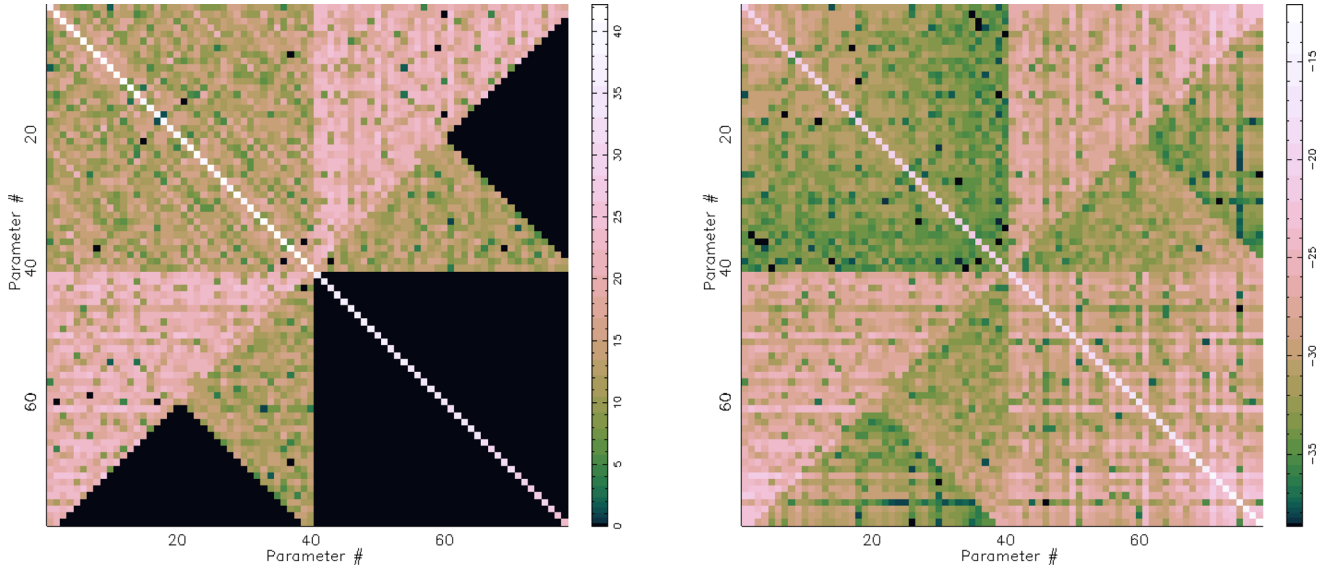

(a) Hessian matrix of the estimated parameters

(b) Covariance matrix of the estimated parameters

Figure 5. The kite plots: panel (a) shows the magnitude of the complex elements of the Hermitian-symmetric Hessian matrix and panel (b) shows the magnitude of the complex elements of the Hermitian-symmetric covariance matrix, both given in decibel($10\log_{10}(.)$) scale to accommodate the large contrast. The matrices are both 78×78 elements across, with the first 40 elements on each side corresponding to the errors on estimated complex antenna gains $\widehat{g}_i$, and the next 38 elements, the errors on the estimated model visibilities $\widehat{M}_{|i-j|}$. The diagonal elements of the matrices are, of course, real. The full range of grey-scale intensity is exploited here using the 'cubehelix' mapping scheme (Green 2011).

calibration algorithms. See e.g. Noordam & Smirnov (2010); Smirnov (2011); Bhatnagar et al. (2008)] to address these issues. A further issue that is relevant in dealing with dipole arrays (as is the case of the focal array at the ORT) is that there could be mutual coupling between the elements. Addressing these issues for the ORT is beyond the scope of the current paper, but we plan to return to these in future work. We discuss below some considerations which suggest that the approximations that we have made are reasonable to first order for the problem at hand. First, the ORT measures only the polarization along the length of the telescope, i.e. north–south. The dipoles are hence arranged end to end, a configuration that one would intuitively expect to minimize mutual coupling. Indeed measurements of the sensitivity indicate that the sensitivity of the ORT increases linearly with the number of dipole signals added, again suggesting that the mutual coupling can be ignored to first order. Further since the ORT is equatorially mounted, the beams do not rotate in the sky as it tracks the source, and hence to the extent that the different sections have identical beams, the calibration issues are greatly simplified. Interestingly, this means that the baseline lengths will also be fixed as it tracks the source, meaning that each element pair measures the same sky visibility at all times. Finally, since the 'array' is small (530m), Phase I of the upgrade (which breaks the array up into 40 elements) falls within Lonsdale's regime 1 (Lonsdale 2005), where the traditional solution to the ionospheric phase suffices. Phase II, where every 2 m segment of the telescope will be digitized (i.e. a compact array, wide field of view, although note that even in this case, the east–west field of view is limited to 2° because of the reflector) would fall into Lonsdale's case 3, where each source in the field of view could be shifted by a time variable offset, that would need to be calibrated for. We note that the NLS algorithm suggested above would also be useful to quantify the importance of effects. Residuals (obtained after calibration as described here) between the visibilities measured on nominally redundant baselines would be indicative of the importance of the direction dependent effects.

5 CONCLUSIONS

We apply a standard iterative NLS minimization algorithm (i.e. steepest descent) to the problem of redundancy calibration. We apply this method to simulated data; the simulations were done in the context of the ongoing upgrade of the ORT. We find that the NLS algorithm is fast and accurate compared to the LLS methods that have been used in the past. The linear method works with the logarithm of the antenna gains and the sky visibilities, and hence leads to biased estimates of these parameters even at modest SNRs. Linearization using a Taylor expansion of the logarithm in the equations used in the linear method has been proposed to circumvent this problem. In comparison to this, we find that the NLS algorithm is fast as well as simple to implement. We also investigate the accuracy of the estimates obtained by the NLS algorithm and find from a Monte Carlo simulation that the ensemble parameter errors attain the CRB at moderate SNRs.

ACKNOWLEDGEMENTS

The authors wish to thank Mihir Arjunwadkar (NCRA/CMS), Shiv Sethi (RRI) and Rajaram Nityananda (NCRA) for many useful discussions and inputs. They also thank C R Subrahmanya (RRI), Peeyush Prasad (ASTRON) and P K Manoharan (RAC) for their help during the course of this work. We owe our many thanks to the engineering support staff at RAC, Ooty for their contribution to the design and installation of the receiver. The authors wish to thank Jan Noordam for his comments which have helped improve this paper significantly.

REFERENCES

Bhatnagar S., Cornwell T. J., Golap K., Uson J. M., 2008, A&A, 487, 419
Cornwell T. J., Fomalont E. B., 1999, in Taylor G. B., Carilli C. L., Perley R. A., eds, ASP Conf. Ser. Vol. 180, Synthesis Imaging in Radio Astronomy II. Astron. Soc. Pac., San Francisco, p. 187

Falcke H. et al., 2006, High. Astron., 14, 119
Green D. A., 2011, Bull. Astron. Soc. India, 39, 289
Hamaker J. P., 2000, A&AS, 143, 515
Liu A., Tegmark M., Morrison S., Lutomirski A., Zaldarriaga M., 2010, MNRAS, 408, 1029
Lonsdale C. J., 2005, in Kassim N., Perez M., Junor M., Henning P., eds, ASP Conf. Ser. Vol. 345, From Clark Lake to the Long Wavelength Array. Astron. Soc. Pac., San Francisco, p. 399
Lonsdale C. J. et al., 2009, Proc. IEEE, 97, 1497
Noordam J. E., de Bruyn A. G., 1982, Nat, 299, 597
Noordam J. E., Smirnov O. M., 2010, A&A, 524, A61
Noorishad P., Wijnholds S. J., van Ardenne A., van der Hulst J. M., 2012, A&A, 545, A108
Parsons A., Pober J., McQuinn M., Jacobs D., Aguirre J., 2012, ApJ, 753, 81
Peterson J. B., Bandura K., Pen U., 2006, preprint (astro-ph/0606104)
Pober J. C. et al., 2012, AJ, 145, 65
Poor H. V., 1994, An Introduction to Signal Detection and Estimation, 2nd edn. Springer-Verlag, Berlin
Prasad P., Subrahmanya C. R., 2011, Exp. Astron., 31, 1
Press W. H., Teukolsky S. A., Vetterling W. T., Flannery B. P., 1992, Numerical Recipes in C – The Art of Scientific Computing, 2nd edn. Cambridge Univ. Press, Cambridge
Rengelink R. B., Tang Y., de Bruyn A. G., Miley G. K., Bremer M. N., Roettgering H. J. A., Bremer M. A. R., 1997, A&AS, 124, 259
Smirnov O. M., 2011, A&A, 527, A107
Swarup G. et al., 1971, Nat. Phys. Sci., 230, 185
Thompson A. R., Moran J. M., Swenson G. W., Jr, 2001, Interferometry and Synthesis in Radio Astronomy, 2nd edn. Wiley, New York
Wieringa M., 1991, PhD thesis, Rijksuniversiteit te Leiden
Wieringa M., 1992, Exp. Astron., 2, 203
Wijnholds S. J., 2010, PhD thesis, Technische Universiteit Delft
Wijnholds S. J., Noorishad P., 2012, Proc. 20th EuSiPCo., Statistically Optimal Self-Calibration of Regular Imaging Arrays. IEEE, Piscataway, p. 1304

This paper has been typeset from a TEX/LATEX file prepared by the author.